Journal of ELECTRONIC MATERIALS, Vol. 38, No. 4, 2009
DOI: 10.1007/s11664-009-0672-z

GaN Nanowire Carrier Concentration Calculated from Light and Dark Resistance Measurements

L.M. MANSFIELD,[1,2] K.A. BERTNESS,[1] P.T. BLANCHARD,[1] T.E. HARVEY,[1] A.W. SANDERS,[1] and N.A. SANFORD[1]

1.—Optoelectronics Division, National Institute of Standards and Technology, Boulder, CO, USA.
2.—e-mail: lorelle@boulder.nist.gov

We obtained the carrier concentration and mobility of silicon-doped gallium nitride nanowires at room temperature with light and dark resistance data. Current–voltage measurements were performed on single-nanowire devices in the dark and under 360 nm illumination. Field-emission scanning electron microscopy was used to measure the device dimensions. The nanowires were modeled with cylindrical geometry, and solutions were computed with a nonlinear fit algorithm. Simulations were also performed to verify the model. The carrier concentration was bounded by 6×10^{17} cm^{-3} and 1.3×10^{18} cm^{-3}, and the mobility was between 300 cm^2 V^{-1} s^{-1} and 600 cm^2 V^{-1} s^{-1}.

Key words: FETs, field-effect transistors, gallium nitride, mobility, nanostructures

INTRODUCTION

GaN nanowires are being investigated for a variety of applications[1] from biosensors to field-effect transistors (FETs)[2,3] to ultraviolet (UV) laser diodes.[4] They could also be an alternative to thin films in high-power and high-frequency electronics. Our nanowires, grown by plasma-assisted molecular-beam epitaxy (PAMBE), are well suited to these devices because they have high crystalline quality.[5–7] While researchers are well on the way to refining the growth and processing steps required for these devices, measurement of the material properties of nanowires has not been perfected.

It is important that additional methods for nanowire characterization be developed. Simple resistance and depletion region models are difficult to apply to *c*-axis GaN nanowires because of their small size and hexagonal cross-sections. Traditional thin-film techniques such as Hall measurements may not be possible on the nearly one-dimensional geometry of nanowires. Carrier concentration and mobility calculations are also complicated, because the two parameters are interrelated. Capacitance–voltage measurements have recently been performed on arrays of nanowires[8] and FET measurements are widely used to extract nanowire properties.[1,2,9–16] However, the accuracy of the nanowire FET model is still in question,[16,17] and errors of factors of ten or more are possible. Therefore, additional measurement techniques are necessary for comparison with and verification of the currently used methods.

We have determined the carrier concentration and mobility for a group of GaN nanowires from a single growth run using resistance measurements with and without UV illumination. Resistance measurements were performed on four-terminal and two-terminal devices with ohmic contacts. We used a nonlinear fit of the dark and UV resistance data to extract the carrier concentration and mobility, and included corrections for the transfer length and depletion width of the nanowires. The model was verified with several simulations, and results were compared with field-effect transistor measurements. This method provides values of carrier concentration and boundaries on nanowire mobility. It applies to nanowire batches for which there is a reasonable expectation of material uniformity in electrical properties.

(Received August 5, 2008; accepted January 13, 2009; published online January 30, 2009)

EXPERIMENT

Gallium nitride nanowires were grown by plasma-assisted molecular-beam epitaxy on silicon (111) substrates. Our nanowires grow perpendicular to the substrate in the *c*-axis direction and have hexagonal cross-sections. Details of the growth procedure can be found elsewhere.[18–20] For this experiment, silicon was introduced during the GaN growth process. Silicon is a known *n*-type dopant in GaN, and the resulting nanowires were doped and conductive as confirmed by current–voltage measurements. At 1 V bias, devices made from undoped nanowires have currents in the low 10^{-9} A range, compared with currents in the 10^{-5} A range or even higher for Si-doped nanowires at the same bias. The nanowires were typically $\sim$15 μm long and had average diameters between 200 nm and 300 nm. Some nanowires were found with diameters outside of the average range and were specifically chosen for this experiment.

We fabricated four-point devices from single GaN nanowires. Pieces of the as-grown material were placed in isopropanol and ultrasonically agitated to remove the nanowires from the growth substrate. The resulting nanowire suspension was dispersed via pipette onto a Si wafer with a 100-nm SiO_2 wet oxide grown at 1000°C. After the solvent evaporated, the nanowires were left behind with enough surface adhesion to remain in place during photolithographic patterning. The exposed sections of the nanowires were cleaned with a reactive-ion etch (30 W, 20 Pa, 20 s, O_2 at 75 sccm) to remove organic contaminants. Metal pads were fabricated with 20 nm of Ti and 200 nm of Al deposited by electron-beam evaporation followed by an acetone liftoff. The samples were annealed at 500°C for 60 s in a 5% H_2/95% Ar ambient to form ohmic contacts. This recipe was previously shown to make ohmic contacts to *n*-type GaN films.[21]

Device dimensions were obtained with field-emission scanning electron microscopy (FESEM). The FESEM image in Fig. 1 shows a typical four-point device. We measured the nanowire diameter on both sides of each contact. The nanowire length between contacts and the contact lengths were also recorded.

Current–voltage (*I–V*) measurements were taken for each working device. Two-point resistance values were calculated from the *I–V* curves by taking the inverse slope of a line fit through zero. The *I–V* curves were linear, with all of the devices used here showing ohmic contact behavior. Control measurements were also performed to ensure that contacts without a spanning nanowire were electrically isolated. In addition to every two-terminal combination, four-point collinear *I–V* measurements were obtained. The collinear resistance, $R_{\text{collinear}}$, was measured by driving current through the outer two leads and measuring the voltage between the inner two leads. This strategy for isolating the contact resistance was insufficient, however, because of the unusual geometry of the nanowires, and will be discussed in detail below.

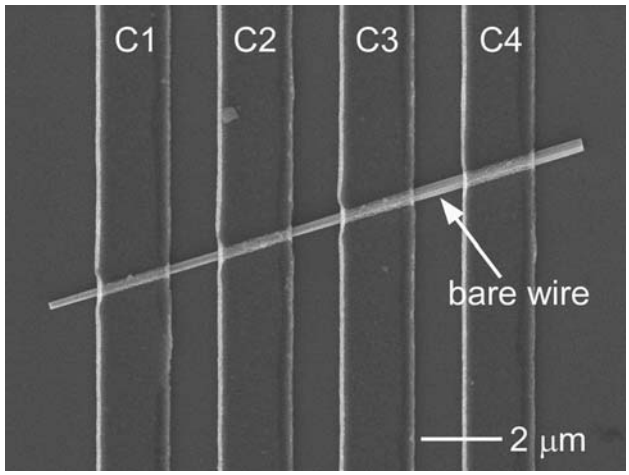

Fig. 1. Top-view FESEM image of a typical four-point device. C1, C2, C3, and C4 are the Ti/Al contact leads. Four-point collinear resistance was measured by driving current through the outer two leads, C1 and C4, measuring the voltage between the inner two leads, C2 and C3. Two-terminal measurements were made by applying voltage and measuring current on adjacent contacts.

In addition to the four-terminal measurements, we took two-terminal *I–V* measurements in the dark and under ultraviolet (UV) illumination on the same devices. For this portion of the experiment, we chose two-terminal combinations that spanned a variety of nanowire radii. Measurements were taken at room temperature, and maximum bias voltages were 3 mV to 7 mV. The UV measurements were performed under steady-state illumination at 360 nm wavelength supplied by a 75-W Xe arc lamp with a monochromator. UV light was focused on the sample with fused-silica optics. The resulting beam had an approximate intensity of 3.6 mW/cm^2 and a spot size of approximately 1 mm diameter, which is approximately 100 times greater than the nanowire length. Dark *I–V* measurements were taken inside a closed black box. Since they display persistent photoconductivity, nanowire samples were placed in the dark for at least 15 h before dark *I–V* scans were performed. During the time between 2 h in the dark and 15 h in the dark, the current in average-sized nanowires fell 3% to 4%, but the current in small-diameter nanowires fell as much as 20%. Device resistances in the dark and under illumination were calculated from the inverse slope of a line fit through zero on the *I–V* curves. Resistance values were repeatable, with measurements of the same device made on different days varying by less than 0.6%. Table I lists the resistance values along with the dimensions of the two-terminal nanowire devices.

Photocurrent measurements were taken at various UV intensities using the apparatus described above. The power intensity of the lamp dropped

Table I. Measurements of Two-Terminal Nanowire Devices

Device	R_{dark} (Ω)	R_{uv} (Ω)	r_m (nm)	L_{nw} (nm)	L_{c1} (nm)	L_{c2} (nm)
1	954,900	132,200	48	1950	245	1820
2	17,090	10,800	122	1260	1940	1900
3	29,440	17,680	122	1905	1495	1585
4	17,320	11,640	138	1655	1710	1760
5	22,810	14,910	152	3585	2385	2385
6	15,500	9458	156	1555	1625	1620
7	12,590	8948	158	2100	2175	2110
8	14,730	9405	160	2045	1545	1520
9	9274	6615	168	1620	1610	1600
10	10,060	6809	178	1595	1620	1620
11	5371	3967	274	1700	1675	1685
12	3696	3045	328	2025	2290	2285

Devices are sorted by radius from smallest to largest. R_{dark} is the nanowire resistance obtained from the *I–V* curve taken in the dark, R_{uv} is the nanowire resistance under UV illumination, r_m is the average measured radius of the nanowire rounded to the nearest even number, L_{nw} is the length of the nanowire between the contacts, L_{c1} is the length of nanowire covered by contact 1, and L_{c2} is the length of the nanowire covered by contact 2. Length measurements were rounded to the nearest 5 nm.

from 3.6 mW/cm^2 to approximately 2.7 mW/cm^2 between the *I–V* measurements taken at 100% illumination and the photocurrent measurements. Fused-silica neutral-density filters were placed between two of the lenses before the light was focused on the sample. Combinations of filters were used to attenuate the intensity, spanning almost five orders of magnitude. At each UV intensity, the devices were set at a constant bias voltage and a current reading was taken every second for at least half an hour. Figure 2a shows two typical photocurrent scans. The first jump in current occurs when the light is allowed onto the sample. Variation in current that occurs after 300 s is due to fluctuations in the Xe lamp intensity. Photocurrent data presented in Fig. 2b is the average photocurrent taken from 500 s to the end of the scan. Notice that the photocurrent begins to level off at 50% of the UV power intensity, showing that the surface band bending in the nanowire is nearing 0 V.

On several of the devices, back-gated FET measurements were performed under local atmospheric pressure (Boulder, CO, USA) in air. Gate voltage was applied through the conductive silicon substrate with silver paint as a back contact. The Ti/Al metal pads fabricated earlier were used as source and drain contacts. The devices displayed channel current modulation as the gate bias was varied from −35 V to 35 V, while the drain–source voltage was held constant at values from 0.1 V to 1 V. Consecutive forward and backward sweeps of gate voltage revealed noticeable hysteresis in all of the devices tested.

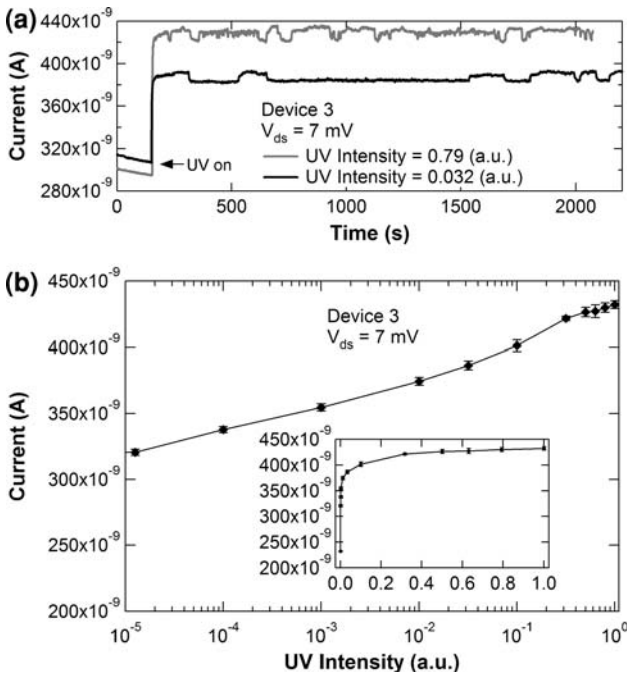

Fig. 2. (a) Two typical photocurrent versus time scans taken at a drain–source voltage of 7 mV. The grey scan is at 79% UV power intensity and the black scan is at 3.2% UV power intensity. The first jump in current occurs when the light is allowed onto the sample. Variation in current that occurs after 300 s is due to fluctuations in the Xe lamp intensity. (b) Photocurrent versus UV power intensity. The photocurrent data presented is the average photocurrent, in scans similar to (a), taken from 500 s to the end of the scan. The inset shows the same data with the UV power intensity on a linear scale. Notice that the photocurrent begins to level off at 50% of the UV power intensity, showing that the surface band bending in the nanowire is nearing 0 V. Two terminal *I–V* measurements taken under illumination were all performed with 100% of the UV power intensity.

DISCUSSION

Carrier concentration and mobility for nanowires are sometimes obtained from nanowire FET measurements, but the standard equations often use assumptions that do not fit most nanowire devices and thus introduce large systematic errors. Typically the gate–nanowire capacitance is calculated with

$$C = \frac{2\pi L_{nw}\varepsilon_o\varepsilon_{ox}}{\ln(2t_{ox}/r_m)}, \quad (1)$$

where L_{nw} is the length of the nanowire, $\varepsilon_o = 8.854 \times 10^{-14}$ F/cm, ε_{ox} is the dielectric constant of the oxide, t_{ox} is the oxide thickness, and r_m is the nanowire radius. This method assumes that the nanowire is encased in oxide, so Wunnicke[16] suggests changing the oxide dielectric constant, ε_{ox}, from 3.9 for silicon dioxide, to an effective dielectric constant of 2.2. The dielectric constant change immediately cuts the capacitance almost in half. In Eq. 1, the oxide thickness is assumed to be much greater than the nanowire radius, which was not true in our case. Removing this assumption takes the capacitance calculation back to

$$C = \frac{2\pi L_{nw}\varepsilon_o\varepsilon_{ox}}{\cosh^{-1}((r_m + t_{ox})/r_m)} \quad (2)$$

and can easily result in more than fivefold reductions in capacitance for devices with nanowires of large radius and thin oxide layers, in other words, as r_m approaches $2t_{ox}$.[17] The capacitance error propagates causing an artificially high carrier concentration, $N_d = \frac{V_{th}C}{q\pi(r_m)^2 L_{nw}}$, and an artificially low mobility, $\mu = \frac{g_m}{V_{ds}}\frac{L_{nw}^2}{C}$, where V_{th} is the threshold voltage, g_m is the maximum transconductance, and V_{ds} is the drain–source voltage.

Using the standard FET analysis, the average mobility of our nanowires was 32 $cm^2\ V^{-1}\ s^{-1}$ and the average carrier concentration was 1.7×10^{18} cm^{-3}. After applying corrections for the effective dielectric constant and the thickness of the oxide compared with the nanowire radius, the average mobility increased five times to 160 $cm^2\ V^{-1}\ s^{-1}$ and the average carrier concentration fell to 4.7×10^{17} cm^{-3}. FET measurements, for tested devices that showed channel pinch-off and with Eq. 2 for capacitance, are detailed in Table II. Although wire-to-wire differences in carrier concentration and mobility of almost an order of magnitude were observed, the variation was not a function of nanowire diameter. For nanowires from the same growth run, the range of carrier concentrations obtained from FET measurements was 1.5×10^{17} cm^{-3} to 1.3×10^{18} cm^{-3}, which was larger than the carrier concentration range obtained from the model described below.

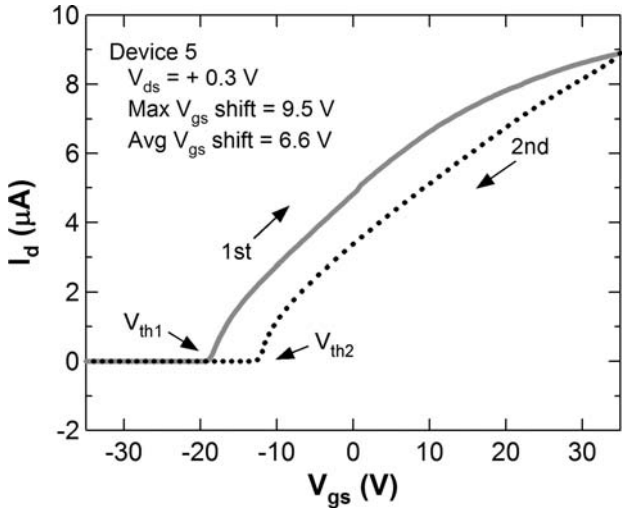

Fig. 3. A gate voltage sweep showing hysteresis at constant drain–source bias, V_{ds}, of 0.3 V for a nanowire FET. The current, I_d, at a given gate voltage, V_{gs}, varied depending on the direction of the sweep. Two different threshold voltages could be calculated from the two curves, which would result in different values for carrier concentration and mobility. The maximum gate voltage shift is 9.5 V and the average gate voltage shift is 6.6 V.

In addition, the FET measurements were not reproducible. Hysteresis and drift were displayed by the FET devices. In a gate voltage sweep at constant drain–source bias, V_{ds}, the current at a given gate voltage varied depending on the direction of the sweep. Figure 3 shows a gate voltage sweep at V_{ds} of 0.3 V with an average gate voltage offset of 6.6 V. The forward scan ran first, followed immediately by the backward scan. As shown in the figure, two different threshold voltages could be calculated from the two curves, which would result in different values for carrier concentration and mobility. Consecutive measurements on the same device but with a slower scan speed also gave different results.

Table II. Back-Gated FET Measurements of Two-Terminal Nanowire Devices

Device	r_m (nm)	C (fF)	V_{th} (V)	g_m (nS)	N_d (cm^{-3})	μ ($cm^2\ V^{-1}\ s^{-1}$)
1	48	0.13	−22	76	1.3×10^{18}	34
2	122	0.13	−30	770	4.1×10^{17}	170
3	122	0.19	−14	700	1.9×10^{17}	270
5	152	0.40	−29	150	2.8×10^{17}	65
8	160	0.24	−16	820	1.5×10^{17}	270

Device numbers match those in Table I. r_m is the measured radius, C is the capacitance calculated with Eq. 2, V_{th} is the gate threshold voltage found by extrapolating the linear region around the point at g_m in the I_d versus V_{gs} graph to $I_d = 0$, g_m is the maximum transconductance ($\partial I_d/\partial V_{gs}$), N_d is the carrier concentration, and μ is the mobility. The range of carrier concentration calculated with our model was from 6×10^{17} cm^{-3} to 1.3×10^{18} cm^{-3} and the mobility was between 300 $cm^2\ V^{-1}\ s^{-1}$ and 600 $cm^2\ V^{-1}\ s^{-1}$.

By simply changing the gate voltage scan speed for one example device, the mobility value increased over 30% from 187 $cm^2\ V^{-1}\ s^{-1}$ with a continuous scan to 248 $cm^2\ V^{-1}\ s^{-1}$ with a scan speed of 0.5 s per point. Some of the inconsistency might be caused by charge trapping due to condensation, since the measurements were made in air rather than in vacuum, but some surface charge trapping would also occur in vacuum. Similar hysteresis has been observed in other GaN FET experiments,[2,9,14] and they propose that it is due to charge trapping in the gate oxide. Regardless of the mechanism, accumulated charge shifts the effective threshold voltage, which results in inconsistent values for carrier concentration and mobility.

We suspect that there are other fundamental problems with the FET measurements. One concern is that the capacitance was originally derived from a model using an infinitely long metal wire,[22] which does not allow for depletion effects in the semiconductor nanowire. Trapped charges at the nanowire–oxide interface and contact resistance are also not considered in the model. A full analysis of errors and their causes is beyond the scope of this paper. The inconsistencies in the FET model prompted us to develop a new model based on simple resistance measurements taken in the dark and under illumination.

MODEL

In order to fit a carrier concentration and mobility to the resistance data, we made several assumptions. As with any model, the degree to which the model fits the data is a test of the assumptions of the model. First, we assumed that nanowires from the same growth run had the same carrier concentration and mobility, and that carrier concentration and mobility are material properties that do not change with exposure to illumination. When electron–hole pairs are created during illumination, the hole density remains orders of magnitude lower than the electron density because many are swept toward the nanowire surface and trapped by the negative surface charges. Therefore, the resistance and the corresponding mobility are affected only by the electrons. Mobility and carrier concentration may vary slightly from wire to wire, but fitting with a single value should yield the average of these values for the group of nanowires. As mentioned earlier, the random variation in resistance measurements was 1%. Next, contact resistivity was given a value of $1 \times 10^{-5}\ \Omega\ cm^2$, since this value is commonly reported for nanowire devices.[23,24] FESEM measurements were repeatable within ±10 nm; therefore we assumed a variation of ±10 nm in length and ±5 nm in radius. We accounted for the uncertainty in nanowire measurements by repeating the fit using the low values for length and radius, and again using the high values for length and radius. Each nanowire radius was one-half of the average diameter measured at the contacted ends. Radius values were modified to approximate the nanowire cross-section as a circle inscribed within a hexagon whose point-to-point diameter was measured as shown in Fig. 4a. This cylindrical geometry was used for the calculations.

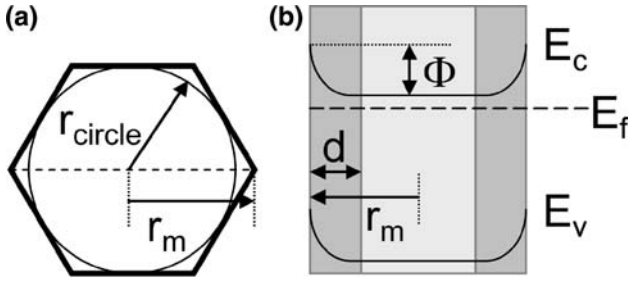

Fig. 4. (a) Hexagonal cross-section of a nanowire. The dotted line represents the diameter measured by FESEM. One-half of the diameter is the measured radius, r_m, which is modified in the model to equal the inscribed radius, r_{circle}. (b) Diagram illustrating the depletion width and surface band bending for a cylindrical nanowire in the dark at equilibrium. The nanowire radius is r_m. The depletion width, d, is shown shaded in the diagram. Conduction occurs through the channel with a radius of $(r_m - d)$. The surface band bending, Φ, is the difference between the conduction band in the undepleted region and the conduction band at the nanowire surface.

Depletion width was also considered in our model. Since there is negative surface charge on the nanowires, a portion of the semiconductor will be depleted of charges, and current will not flow through the entire nanowire, as shown in Fig. 4b. The cross-sectional area, A_{xs}, in the nanowire resistance calculation,

$$R_{nw} = \frac{\rho_s L_{nw}}{A_{xs}}, \tag{3}$$

needs to be modified to account for this depletion width. Equation 3 then becomes

$$R_{nw} = \frac{\rho_s L_{nw}}{\pi (r_m - d)^2}, \tag{4}$$

where ρ_s is the semiconductor (nanowire) resistivity, L_{nw} is the nanowire length, and r_m is the nanowire radius. We calculated the depletion width, d, using an equation for the surface band bending, Φ, that was derived by use of cylindrical symmetry and Gauss's law.[25]

$$\Phi = \frac{qN_d}{2\varepsilon}\left[\frac{r_m^2 - (r_m - d)^2}{2} - (r_m - d)^2 \ln\left(\frac{r_m}{r_m - d}\right)\right]. \tag{5}$$

In this equation, $q = 1.602 \times 10^{-19}$ C, N_d is the carrier concentration, and $\varepsilon = \varepsilon_0 \varepsilon_r$, where $\varepsilon_0 = 8.854 \times 10^{-14}$ F/cm and $\varepsilon_r = 8.9$.[26] Typical depletion widths in the dark were around 25 nm for these Si-doped nanowires. Illuminating the nanowires with ultraviolet light above the band gap decreases the depletion width. Photogenerated carriers partially neutralize the surface states, reducing the

surface band bending and opening the conducting channel in the nanowire. The illuminated resistance values were around 70% of the original measurement for average-sized nanowires. For the smallest-diameter nanowire, however, the illuminated resistance value was only 14% of the dark resistance measurement.

Fitting the data to obtain carrier concentration and mobility values was complicated because the two parameters are related by $\rho_s = \frac{1}{qN_d\mu}$, where μ is the mobility. Rather than solving a simple linear system of n equations and n unknowns, getting solutions for these two coupled values required a nonlinear fit to the data. We made some initial guesses for N_d and μ that were used as starting values in the fitting routine, and fixed the value of the surface band bending within each fit. Then the device resistance, R_{device}, was calculated based on those starting values:

$$R_{device} = R_{nw} + R_{contact1} + R_{contact2}. \quad (6)$$

Nanowire resistance was modeled using Eq. 4 along with Eq. 5 to account for the depletion width. Contact resistance was calculated using the transfer length correction explained later in Eq. 7.

A Levenberg–Marquardt[27] nonlinear least-squares fitting routine was used to solve simultaneously for the carrier concentration and mobility that provided the best fit to the entire data set, including both dark and illuminated resistances. Inputs to this routine were initial guesses for the fitting parameters N_d and μ, constants for both surface band bending values, and the nanowire dimensions. The device resistances were computed as described above and summarized in Eq. 6. Each modeled resistance was compared with the actual measured resistance via the chi-squared parameter, $\sum_{i=1}^{n}\left(\frac{y-y_i}{\sigma_i}\right)^2$, where y is the modeled device resistance, y_i is the measured device resistance, and σ_i is the standard deviation of the measured resistance. The algorithm then chose new values of N_d and μ, and the process repeated. Iterations continued until chi-squared was minimized. The resulting N_d and μ, along with their uncertainties, were solutions to the experimental data.

We ran the routine several times, varying surface band bending in the dark from 0.3 V to 0.7 V and surface band bending under illumination from 0 V to 0.05 V. The actual surface band bending for our GaN nanowires is unknown. For nanowire devices measured in the dark, we chose values within the literature range of 0.1 V to 1.1 V.[28–30] Surface band bending for illuminated nanowires was much lower. The intention was to reduce the surface band bending to 0 V, but since this could not be confirmed, a range of low values was used. Figure 2b does show, however, that the nanowires are tending toward the flat-band condition under UV illumination. The inset clearly shows that the current versus

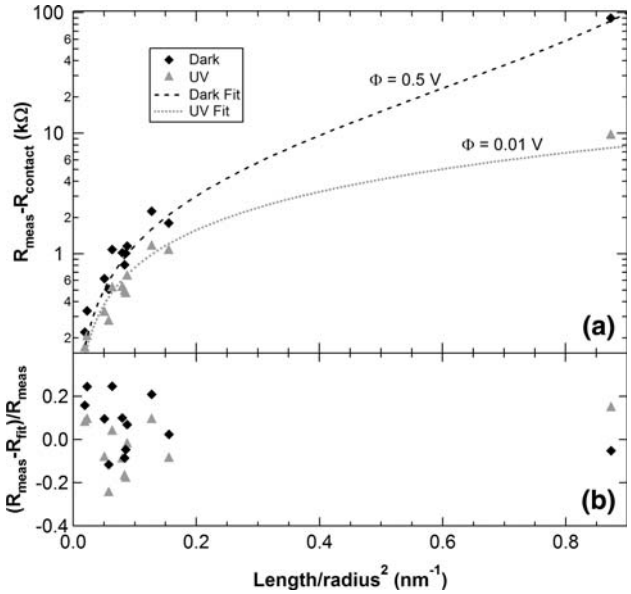

Fig. 5. (a) The measured resistance, R_{meas}, minus the modeled contact resistance, $R_{contact}$, versus length/radius^2 on a log–linear scale. The lines are the model values calculated with surface band bending in the dark at 0.5 V, surface band bending under illumination at 0.01 V, a carrier concentration of 7.8×10^{17} cm^{-3}, and a mobility of 470 cm^2 V^{-1} s^{-1}. (b) The fractional difference for each point, $(R_{meas} - R_{fit})/R_{meas}$, where R_{fit} is the modeled resistance. Modeled resistance values were within 25% of the measured resistance values.

UV intensity begins to level off at around 50% power intensity. Also note that average-sized nanowires still have a depletion width of around 3.6 nm when the surface band bending is 0.01 V and the carrier concentration is 7.8×10^{17} cm^{-3}. Additional studies are underway to obtain experimental values for surface band bending, and they will be reported at a later time.

The model provides a good fit to the data. The points in Fig. 5a show the measured resistance, R_{meas}, minus the modeled contact resistance, $R_{contact}$, versus length/radius^2 on a log–linear scale. The lines are the model values calculated with surface band bending in the dark at 0.5 V and surface band bending under illumination at 0.01 V. Based on a carrier concentration of 7.8×10^{17} cm^{-3} and a mobility of 470 cm^2 V^{-1} s^{-1}, all modeled resistance values were within 25% of the measured resistance values. Figure 5b shows the fractional difference for each point, $(R_{meas} - R_{fit})/R_{meas}$, where R_{fit} is the modeled resistance. This proves that the change in resistance between nanowires kept in the dark and nanowires that are illuminated with UV can be explained by the difference in the size of the conducting channel. Using the above parameters, the diameter of the conducting channel in the dark is 78% to 85% of the conducting channel under UV illumination for average-sized nanowires. Whether the current is confined to an inner core of the nanowire or is spread throughout most of

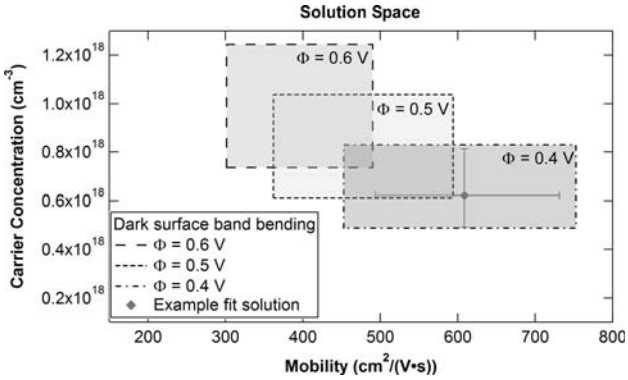

Fig. 6. Solution space of carrier concentration versus mobility. The area inside each rectangle represents solutions for the carrier concentration and mobility of the group of nanowires for a given surface band bending in the dark. Included in the space are the uncertainty in measured nanowire dimensions and variation in surface band bending under illumination from 0 V to 0.05 V. The point with error bars is an example fit solution for surface band bending in the dark of 0.4 V and surface band bending under illumination of 0.01 V. Each rectangle contains six points similar to the one shown, and each point is a solution for a given value of surface band bending under illumination. Note that the solution-space shape is not actually a perfect rectangle.

the nanowire diameter, the values of carrier concentration and mobility do not change dramatically. Figure 5b confirms that our model fits the resistance data and therefore our earlier assumptions were reasonable.

The results of the many fit iterations were constructed into a solution-space graph shown in Fig. 6. The shapes of the solution spaces are more complicated than shown in the figure, but the rectangles provide a good visual representation of the extent of each solution space. The area inside each rectangle represents solutions for the carrier concentration and mobility of the group of nanowires at a given surface band bending in the dark. Included in the solution space are multiple fit results obtained by changing the nanowire dimensions based on the measurement uncertainty, and by varying the surface band bending under illumination from 0 V to 0.05 V.

The procedure described does not converge on a single unique solution for carrier concentration and mobility, because of the nonlinear interrelatedness of the two parameters. The fitting algorithm returns an uncertainty associated with each parameter, and the magnitude of this uncertainty increases with the uncertainty in the nanowire resistance and dimension measurements. One such point with uncertainty bars is illustrated within the $\Phi = 0.4$ rectangle in Fig. 6. Between 97% and 98% of each uncertainty bar is due to uncertainty in the nanowire dimensions. Another way to interpret these uncertainty limits is to say that they represent the range of combinations of carrier concentration and mobility that would fit the data equally well when the fit is constrained to a particular surface band bending value. Even with several data points covering a range of nanowire radii, we find that the range of equally probable carrier concentration and mobility values is on the order of 30% of the average value for these parameters. Our experience also shows that it is easy to find false minima when using a grid search approach rather than the nonlinear curve-fitting algorithm. The full range of equally probable values is only seen when searching in steps on the order of the third significant digit in each parameter.

For this nanowire growth run, the fitting procedure indicated that the carrier concentration was between 6×10^{17} cm^{-3} and 1.3×10^{18} cm^{-3}, and the mobility was between 300 cm^2 V^{-1} s^{-1} and 600 cm^2 V^{-1} s^{-1}. The mobility range was higher than the 150 cm^2 V^{-1} s^{-1} to 250 cm^2 V^{-1} s^{-1} that Fu et al. and others reported for similarly doped, bulk GaN.[31,32] GaN films often have dislocation densities of 8×10^9 cm^{-2}.[32] Transmission electron microscopy (TEM) examination of individual nanowires shows that our MBE-grown nanowires are free of dislocations.[18] Our mobility is higher than most reported nanowire mobilities,[15,33,34] but it is similar to the 300 cm^2 V^{-1} s^{-1} at 2×10^{18} cm^{-3} reported for GaN nanowire FETs by Huang et al.,[1] whose nanowires are also single crystalline and grown in the [100] direction.[35] The elevated mobility range is probably due to the defect-free nature of our material.

One source of systematic uncertainty in our model is imprecise knowledge of the contact resistance. Generally the contact resistance, R_{contact}, can be determined by subtracting the collinear resistance, $R_{\text{collinear}}$, from the two-point resistance between the inner two leads, R_{23}, $R_{\text{contact}} = R_{23} - R_{\text{collinear}}$. Then the contact resistivity can be calculated using the device geometry, $R_{\text{contact}} = \rho_c/(2\pi r_m L_c)$, where ρ_c is the contact resistivity, r_m is the nanowire radius,

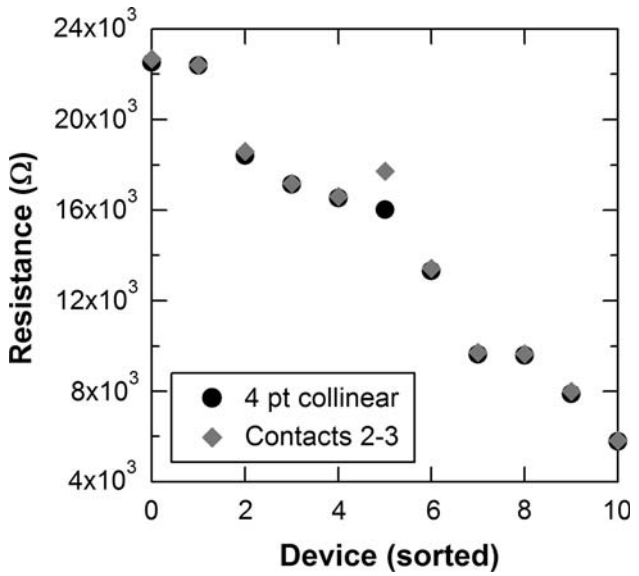

Fig. 7. Measurements of nanowire device resistance between contacts 2 and 3 compared with collinear resistance. Devices are sorted in order of decreasing collinear resistance.

and L_c is the contact length. The graph in Fig. 7 shows that the collinear resistance measurement was nearly identical to the two-point resistance between the inner two leads. In this case the common procedure gave an exceptionally small contact resistivity on the order of 10^{-7} Ω cm^2. Although Yan et al.[21] have produced contacts to GaN film with contact resistivity as low as 10^{-7} Ω cm^2, most reported contact resistivities for GaN films are in the high 10^{-6} Ω cm^2 or low 10^{-5} Ω cm^2 range.[36–38] Nanowire contact resistivities have been reported around 1×10^{-5} Ω cm^2.[23,24]

This discrepancy was resolved by applying a transfer length correction in our model. The transfer length accounts for the distributed current flow near the contact edges. It is discussed in the paper by Mohney et al.[39] and defined as $L_T = \sqrt{\frac{r_m \rho_c}{2F\rho_s}}$, where r_m is the nanowire radius, ρ_c is the contact resistivity, and ρ_s is the semiconductor resistivity. F is the fraction of the nanowire circumference covered by the contact metal, which we estimated from SEM pictures as two-thirds. The transfer length for a nanowire device with an average radius of 125 nm is around 300 nm, which is smaller than our photolithographically defined leads, which are typically 1,500 nm wide. Contact resistance in the model was calculated with the transfer length correction,

$$R_{\text{contact}} = \rho_c \Big/ \left(2\pi r_m L_T F \tanh\left(\frac{L_c}{L_T}\right)\right), \qquad (7)$$

where L_c is the contact length. When we used a contact resistivity of 1×10^{-5} Ω cm^2, the resistance of a typical contact was 2200 Ω.

Another consequence of the short transfer length is that the center metal pads were shunting the nanowire current. We tested this effect by comparing the two-terminal resistance between contacts 1 and 4, R_{14}, and the sum of the two-terminal resistances of the individual wire sections between the pads. Residual resistance is defined as $R_{res} = R_{14} - (R_{12} + R_{23} + R_{34}) - 2R_L$. The thin Ti/Al leads to the nanowire have lead resistances, R_L, on the order of half the difference between R_{23} and $R_{collinear}$. After removing the lead resistance, the residual resistance, R_{res}, was around 1% of the R_{14} resistance. If current was flowing through the nanowire under the metal pads, it is expected that the residual resistance would be substantially higher due to the additional resistance from the lengths of the nanowire underneath the contacts. If the current flows into the center metal pads even when current is supplied through the outer pads, however, the contact resistance of the center pads makes the same contribution to R_{14} as it does to R_{12}, R_{23}, and R_{34}, producing the observed result. The only other possible explanation is that the contact resistance was exactly equal to the resistance of the wire segment underneath it for all nanowires and contacts, which is highly unlikely.

SIMULATIONS

In addition to the data fit described above, we also did several simulations to study how different parameters affected the solution space. Nanowire dimensions were chosen to simulate length, radius, and contact length measurements, and values for carrier concentration, mobility, contact resistivity, surface band bending in the dark, and surface band bending under illumination were set. The resistance of the simulated nanowire devices was calculated with those parameters. Gaussian noise based on a standard deviation of 0.6% of the resistance was added to the resistance numbers to simulate the measurement uncertainty. Finally, we solved for carrier concentration and mobility using the same procedure as was used for the actual data.

By varying one parameter at a time, we were able to isolate its influence on the solution space. In simulation 1, illustrated in Fig. 8, we calculated the resistances that would have resulted from nanowires with the same dimensions as those in our actual data set, but with a lower mobility of 270 cm^2 V^{-1} s^{-1}. The other simulation parameters were a carrier concentration of 5.5×10^{17} cm^{-3}, contact resistivity of 1.0×10^{-5} Ω cm^2, surface band bending in the dark of 0.5 V, and surface band bending under illumination of 0.01 V. Comparing Fig. 8 with Fig. 6 shows that the fitting procedure accurately tracks the change in mobility. The cross on the graph marks the starting values that we used and therefore represents the "actual" solution to the simulated data. In simulation 2, we intentionally overestimated the contact resistivity when we tried to fit the simulated data. Simulated resistance values were constructed by use of 1.0×10^{-6} Ω cm^2 while the contact resistivity in the fitting routine was set to 3.0×10^{-6} Ω cm^2. The higher, incorrect, contact resistivity used in the fit procedure shifted the solution-space graph toward artificially higher mobility values (Fig. 9). Thus, one possible explanation for the higher mobility values we extract

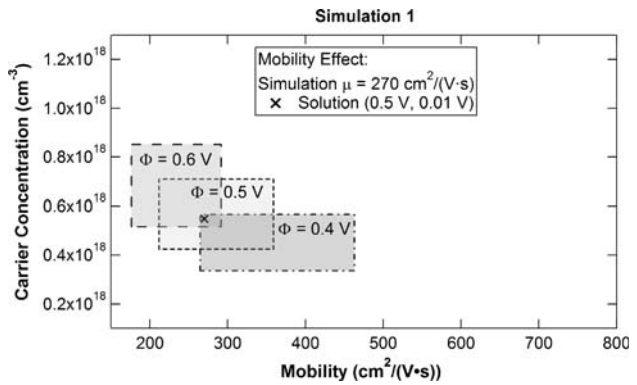

Fig. 8. Graph of the solution space for carrier concentration versus mobility for a simulation with a low starting value of mobility of 270 cm^2 V^{-1} s^{-1}. The starting values are marked with a *cross*.

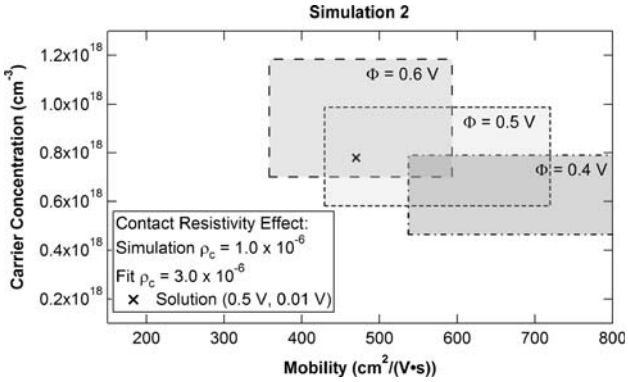

Fig. 9. Graph of the solution space for carrier concentration versus mobility for a simulation where we overestimated the contact resistivity. The simulation values were obtained with $\rho_c = 1.0 \times 10^{-6}$, but the contact resistivity was assumed to be 3.0×10^{-6} for the fit. The starting values are marked with a *cross*.

from our data is that we have overestimated the contact resistivity by a factor of 100 or more. Finally, we note that in simulation 2, nanowire dimensions were simulated that included even more variation in radii than found in our nanowire data set. Because of the nonlinear relationship between carrier concentration and mobility, this greater variability in nanowire radii still led to a large solution space rather than single values for these properties.

Many other insights into the validity of the model were gained through additional simulations. The solution-space graph for the actual data could be reproduced by use of the actual device dimensions and starting values of mobility equal to 470 $cm^2\ V^{-1}\ s^{-1}$ and carrier concentration of $7.8 \times 10^{17}\ cm^{-3}$. Contact resistivity and surface band bending were the same as in the first simulation. We also tried separating effects of nanowire measurement errors. As expected, the size of the solution space rectangle was due mostly to the uncertainty in the nanowire radius rather than to the uncertainty in the nanowire length. Adding more noise to the simulated resistance values did shift and slightly enlarge the solution space, but the actual solution was still included. Changing the surface band bending in the dark had a higher relative effect on the mobility than on the carrier concentration. Mobility solutions shifted to lower values as surface band bending in the dark increased. On the other hand, the solutions shifted to higher values of mobility as assumed surface band bending under illumination increased. Surface band bending in the dark had a much greater effect on the solution space than did surface band bending under illumination. Incremental changes to surface band bending under illumination of 0.01 V led to solutions that overlapped the error bars of the previous solution until the surface band bending under illumination reached approximately 42% of the value for surface band bending in the dark. The starting guesses for mobility and carrier concentration had little effect on the solution space.

SUMMARY

We have calculated a carrier concentration between $6 \times 10^{17}\ cm^{-3}$ and $1.3 \times 10^{18}\ cm^{-3}$ and a mobility between 300 $cm^2\ V^{-1}\ s^{-1}$ and 600 $cm^2\ V^{-1}\ s^{-1}$ for Si-doped GaN nanowires, based on dark and light resistance measurements. *I–V* measurements indicated that we created ohmic contacts to the nanowires, and resistance values were repeatable. A nonlinear fit of the light and dark resistances was used to solve for carrier concentration and mobility. We verified the validity of the calculation method with numerous simulations, and discussed problems in the back-gated FET measurements. Future experiments that will benefit this process are measurements of the surface band bending under light and dark conditions, such as scanning Kelvin probe microscopy, and higher-resolution measurements of nanowire radius. Independent methods for extracting the carrier concentration and mobility of nanowires are also needed to confirm the calculations.

ACKNOWLEDGEMENTS

We thank Ben Klein from Georgia Institute of Technology for simulations showing the shape of the electrical potential for hexagonal nanowires. The studies conducted by the authors from NIST are supported in part by the DARPA Center on Nanoscale Science and Technology for Integrated Micro/Nano-Electromechanical Transducers (iMINT), funded by DARPA N/MEMS S&T Fundamentals Program (HR0011-06-1-0048).

REFERENCES

1. Y. Huang, X.F. Duan, Y. Cui, and C.M. Lieber, *Nano Lett.* 2, 101 (2002). doi:10.1021/nl015667d.
2. H.-Y. Cha, H. Wu, M. Chandrashekhar, Y.C. Choi, S. Chae, G. Koley, and M.G. Spencer, *Nanotechnology* 17, 1264 (2006). doi:10.1088/0957-4484/17/5/018.
3. H.Q. Wu, H.Y. Cha, M. Chandrashekhar, M.G. Spencer, and G. Koley, *J. Electron. Mater.* 35, 670 (2006). doi:10.1007/s11664-006-0118-9.
4. S. Gradecak, F. Qian, Y. Li, H.G. Park, and C.M. Lieber, *Appl. Phys. Lett.* 87, 173111 (2005). doi:10.1063/1.2115087.
5. J.B. Schlager, N.A. Sanford, K.A. Bertness, J.M. Barker, A. Roshko, and P.T. Blanchard, *Appl. Phys. Lett.* 88, 213106 (2006). doi:10.1063/1.2206133.
6. L.H. Robins, K.A. Bertness, J.M. Barker, N.A. Sanford, and J.B. Schlager, *J. Appl. Phys.* 101, 113505 (2007). doi:10.1063/1.2736264.
7. L.H. Robins, K.A. Bertness, J.M. Barker, N.A. Sanford, and J.B. Schlager, *J. Appl. Phys.* 101, 113506 (2007). doi:10.1063/1.2736266.
8. S. Roddaro, K. Nilsson, G. Astromskas, L. Samuelson, L.-E. Wernersson, O. Karlstrom, and A. Wacker, *Appl. Phys. Lett.* 92, 253509 (2008). doi:10.1063/1.2949080.
9. H.Y. Cha, H.Q. Wu, S. Chae, and M.G. Spencer, *J. Appl. Phys.* 100, 4 (2006).
10. S.Y. Lee, T.H. Kim, D.I. Suh, N.K. Cho, H.K. Seong, S.W. Jung, H.J. Choi, and S.K. Lee, *Chem. Phys. Lett.* 427, 107 (2006). doi:10.1016/j.cplett.2006.05.133.
11. A. Motayed, M. Vaudin, A.V. Davydov, J. Melngailis, M.Q. He, and S.N. Mohammad, *Appl. Phys. Lett.* 90, 043104 (2007). doi:10.1063/1.2434153.

12. L. Sang-Kwon, S. Han-Kyu, C. Ki-Chul, C. Nam-Kyu, C. Heon-Jin, S. Eun-Kyung, and N. Kee-Suk, *Mater. Sci. Forum* 527–529, 1549 (2006). doi:10.4028/0-87849-425-1.1549.
13. B.S. Simpkins, P.E. Pehrsson, M.L. Taheri, and R.M. Stroud, *J. Appl. Phys.* 101, 094305 (2007). doi:10.1063/1.2728782.
14. E. Stern, G. Cheng, E. Cimpoiasu, R. Klie, S. Guthrie, J. Klemic, I. Kretzschmar, E. Steinlauf, D. Turner-Evans, E. Broomfield, J. Hyland, R. Koudelka, T. Boone, M. Young, A. Sanders, R. Munden, T. Lee, D. Routenberg, and M.A. Reed, *Nanotechnology* 16, 2941 (2005). doi:10.1088/0957-4484/16/12/037.
15. D. Vashaee, A. Shakouri, J. Goldberger, T. Kuykendall, P. Pauzauskie, and P. Yang, *J. Appl. Phys.* 99, 054310 (2006). doi:10.1063/1.2168229.
16. O. Wunnicke, *Appl. Phys. Lett.* 89, 083102 (2006). doi:10.1063/1.2337853.
17. D.R. Khanal and J. Wu, *Nano Lett.* 7, 2778 (2007). doi:10.1021/nl071330l.
18. K.A. Bertness, N.A. Sanford, J.M. Barker, J.B. Schlager, A. Roshko, A.V. Davydov, and I. Levin, *J. Electron. Mater.* 35, 576 (2006). doi:10.1007/s11664-006-0102-4.
19. K.A. Bertness, A. Roshko, N.A. Sanford, J.M. Barker, and A. Davydov, *J. Cryst. Growth* 287, 522 (2006). doi:10.1016/j.jcrysgro.2005.11.079.
20. K.A. Bertness, A. Roshko, L.M. Mansfield, T.E. Harvey, and N.A. Sanford, *J. Cryst. Growth* 300, 94 (2007). doi:10.1016/j.jcrysgro.2006.10.209.
21. J. Yan, M.J. Kappers, Z.H. Barber, and C.J. Humphreys, *Appl. Surf. Sci.* 234, 328 (2004). doi:10.1016/j.apsusc.2004.05.066.
22. P.M. Morse and H. Feshbach, *Methods of Theoretical Physics*, Vol. 2 (New York: McGraw-Hill Book Company, Inc., 1953), p. 1180.
23. M.-H. Ham, J.-H. Choi, W. Hwang, C. Park, W.-Y. Lee, and J.-M. Myoung, *Nanotechnology* 17, 2203 (2006). doi:10.1088/0957-4484/17/9/021.
24. C. Hwang, J.H. Hyung, S.Y. Lee, C.O. Jang, T.H. Kim, P. Choi, and S.K. Lee, *J. Phys. D Appl. Phys.* 41, 105103 (2008). doi:10.1088/0022-3727/41/10/105103.
25. B.S. Simpkins, M.A. Mastro, J.C.R. Eddy, and P.E. Pehrsson, *J. Appl. Phys.* 103, 104313 (2008). doi:10.1063/1.2932072.
26. E.F. Schubert, *Physical Data for GaN* (Troy, NY: Rensselaer Polytechnic Institute). http://www.rpi.edu/∼schubert/.
27. D.W. Marquardt, *J. Soc. Ind. Appl. Math.* 11, 431 (1963). doi:10.1137/0111030.
28. R. Calarco, M. Marso, T. Richter, A.I. Aykanat, R. Meijers, A. van der Hart, T. Stoica, and H. Luth, *Nano Lett.* 5, 981 (2005). doi:10.1021/nl0500306.
29. S. Chevtchenko, X. Ni, Q. Fan, A.A. Baski, and H. Morkoc, *Appl. Phys. Lett.* 88, 122104 (2006). doi:10.1063/1.2188589.
30. S.A. Chevtchenko, M.A. Reshchikov, Q. Fan, X. Ni, Y.T. Moon, A.A. Baski, and H. Morkoc, *J. Appl. Phys.* 101, 113709/1 (2007).
31. Y. Fu, M. Willander, Z.F. Li, and W. Lu, *Phys. Rev. B* 67, 113313 (2003). doi:10.1103/PhysRevB.67.113313.
32. H.M. Ng, D. Doppalapudi, T.D. Moustakas, N.G. Weimann, and L.F. Eastman, *Appl. Phys. Lett.* 73, 821 (1998). doi:10.1063/1.122012.
33. T. Kuykendall, P. Pauzauskie, S.K. Lee, Y.F. Zhang, J. Goldberger, and P.D. Yang, *Nano Lett.* 3, 1063 (2003). doi:10.1021/nl034422t.
34. S.-K. Lee, H.-J. Choi, P. Pauzauskie, P. Yang, N.-K. Cho, H.-D. Park, E.-K. Suh, K.-Y. Lim, and H.-J. Lee, *Phys. Status Solidi B* 241, 2775 (2004). doi:10.1002/pssb.200404989.
35. X.F. Duan and C.M. Lieber, *J. Am. Chem. Soc.* 122, 188 (2000). doi:10.1021/ja993713u.
36. M.E. Lin, Z. Ma, F.Y. Huang, Z.F. Fan, L.H. Allen, and H. Morkoc, *Appl. Phys. Lett.* 64, 1003 (1994). doi:10.1063/1.111961.
37. J.S. Kwak, S.E. Mohney, J.Y. Lin, and R.S. Kern, *Semicond. Sci. Technol.* 15, 756 (2000). doi:10.1088/0268-1242/15/7/316.
38. L.K. Li, L.S. Tan, and E.F. Chor, *J. Cryst. Growth* 268, 499 (2004). doi:10.1016/j.jcrysgro.2004.04.080.
39. S.E. Mohney, Y. Wang, M.A. Cabassi, K.K. Lew, S. Dey, J.M. Redwing, and T.S. Mayer, *Solid-State Electron.* 49, 227 (2005). doi:10.1016/j.sse.2004.08.006.